Nanoscale

PAPER

View Article Online
View Journal | View Issue

Cite this: *Nanoscale*, 2015, **7**, 2545

Nonradiative energy transfer in colloidal CdSe nanoplatelet films†

Burak Guzelturk,[a,b] Murat Olutas,[a,c] Savas Delikanli,[a] Yusuf Kelestemur,[a] Onur Erdem[a] and Hilmi Volkan Demir*[a,b]

Received 11th October 2014,
Accepted 27th November 2014

DOI: 10.1039/c4nr06003b

www.rsc.org/nanoscale

Nonradiative energy transfer (NRET) has been extensively studied in colloidal nanocrystal (quantum dots) and nanorod (quantum wires) assemblies. In this work, we present the first account of spectroscopic evidence of NRET in solid thin films of CdSe based colloidal nanoplatelets (NPLs), also known as colloidal quantum wells. The NRET was investigated as a function of the concentration of two NPL populations with different vertical thicknesses *via* steady state and time resolved spectroscopy. NRET takes place from the NPLs with smaller vertical thickness (*i.e.*, larger band gap) to the ones with a larger vertical thickness (*i.e.*, smaller band gap) with efficiency up to ~60%. Here, we reveal that the NRET efficiency is limited in these NPL solid film assemblies due to the self-stacking of NPLs within their own population causing an increased distance between the donor–acceptor pairs, which is significantly different to previously studied colloidal quantum dot based architectures for nonradiative energy transfer.

Introduction

Colloidal semiconductor nanoplatelets (NPL), which have strong quantum confinement in one dimension (1D) only, have been recently synthesized in the form of CdE (E = Se, S and Te) with precisely controlled vertical thicknesses.[1,2] These NPLs exhibit unique and favorable optical properties including narrow photoluminescence spectra due to the absence of inhomogenous broadening, splitting of the electron/light–hole and electron/heavy–hole transitions, and giant oscillatory strength resembling their epitaxial counterparts.[2–6] These features differentiate the NPLs from other colloidal semiconductor nanomaterials having different quantum confinement dimensionality such as 3D-confined colloidal nanocrystals (quantum dots) and 2D-confined nanorods (quantum wires). Furthermore, these advantageous properties make the NPLs extremely promising for optoelectronic applications, including LEDs[7] and lasers.[8] To date, CdSe NPLs having a zinc blende crystal structure have been the most extensively studied type among other types of NPLs thanks to their optimized synthetic routes resulting in high quality NPLs with a magic sized vertical thickness with reasonably uniform lateral size distribution.[2,9] The vertical thickness of the NPLs is denoted by the number of monolayers (MLs) of the repeating lattice units. Commonly synthesized vertical thickness of CdSe NPLs range from 3 to 6 MLs. The peak emission wavelength of 3, 4 and 5 ML CdSe NPLs correspond to 463, 513 and 551 nm, respectively, with emission full-width at half-maxima (FWHM) as narrow as 8 nm at room temperature.

Previously, the optical properties of the NPLs have been studied, both in the solution and solid phase. In the case of solid thin films, either ensemble or single NPL based studies have been reported.[4–6,10–13] However, in all of these previous reports only a single population of NPL emitter with a fixed vertical thickness was considered and investigated. On the other hand, it is widely known that nonradiative energy transfer (NRET), also commonly referred to as Förster resonance energy transfer (FRET),[14] can take place within the close-packed assemblies of semiconductor nanostructures (*e.g.*, colloidal nanocrystals and nanorods) with different sizes through near field dipole–dipole coupling.[15–18] Therefore, it is expected to realize NRET in close-packed solid films incorporating NPL populations, each of a different vertical thickness. However, NRET has not been systematically studied nor demonstrated in the solid assemblies of the NPLs to date. In this work, we show the first spectroscopic evidence of NRET within the solid films of CdSe NPLs with vertical thicknesses of 4 and 5 ML. We systematically investigate the NRET as a function of the donor-to-acceptor ratio *via* time-resolved and steady state fluorescence spectroscopy, which conclusively reveal the existence of NRET

[a]*Department of Electrical and Electronics Engineering, Department of Physics, UNAM - Institute of Materials Science and Nanotechnology, Bilkent University, Ankara 06800, Turkey. E-mail: volkan@bilkent.edu.tr, hvdemir@ntu.edu.sg; Fax: +90 312 290-1123; Tel: +90 312 290-1021*

[b]*Luminous! Center of Excellence for Semiconductor Lighting and Displays, School of Electrical and Electronic Engineering, School of Physical and Mathematical Sciences, Nanyang Technological University, Nanyang Avenue, Singapore 639798, Singapore*

[c]*Department of Physics, Abant Izzet Baysal University, Bolu 14280, Turkey*

†Electronic supplementary information (ESI) available: TEM images of the stacked NPLs. See DOI: 10.1039/c4nr06003b

from 4 to 5 ML NPLs. Furthermore, the NRET efficiency was analyzed and found to be limited to ~60%. This limitation was understood by investigating the morphology of the mixed solid thin films, where stacking of the donor and acceptor NPLs within their own population results in a nanoscale phase segregation between the donor–acceptor pairs of the NPLs. This type of phase segregation has not been observed in mixed donor–acceptor pairs of colloidal quantum dots and rods.

Results and discussion

CdSe NPLs with 4 and 5 ML vertical thicknesses exhibiting 30–50% photoluminescence quantum yield were synthesized using a modified recipe and dissolved in hexane (see the Experimental section).[1] The absorption (dashed) and photoluminescence (solid) spectra of the synthesized 4 and 5 ML NPLs are shown in Fig. 1. The absorbance of the NPLs exhibits pronounced sharp features corresponding to the electron/light–hole (480 nm for 4 ML and 518 nm for 5 ML) and the electron/heavy–hole (512 nm for 4 ML and 549 nm for 5 ML) transitions characteristic to the NPLs.[2] During the synthesis of 4 and 5 ML NPLs, quantum dots and/or NPLs with different vertical thickness could possibly be synthesized as a side product. However, using size selective precipitation *via* ultracentrifugation it is possible to totally eliminate these side products. As shown by the absorbance of the NPL solutions after size selective precipitation in Fig. 1, there is no contribution from the side products. Therefore, we were able to achieve NPL solutions containing only a single NPL population. In these NPLs, radiative recombination takes place at the electron/heavy–hole transition resulting in the peak emission wavelength at 513 nm from 4 ML NPLs and 551 nm from 5 ML NPLs, both with FWHM of ~8 nm as shown in Fig. 1.

High-angle annular dark field transmission electron microscopy (HAADF-TEM) was utilized to image the 4 and 5 ML NPLs on carbon coated ultrathin copper grids as shown in Fig. 2a and 2b, respectively. The average size of the 4 ML NPLs

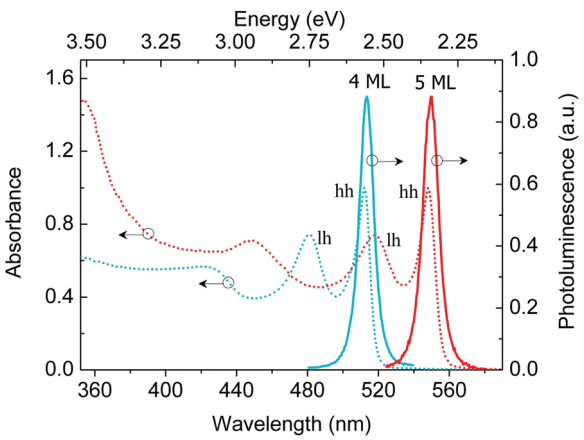

Fig. 1 Absorption (dashed lines) and photoluminescence (solid lines) of the 4 ML (cyan) and 5 ML (red) NPLs.

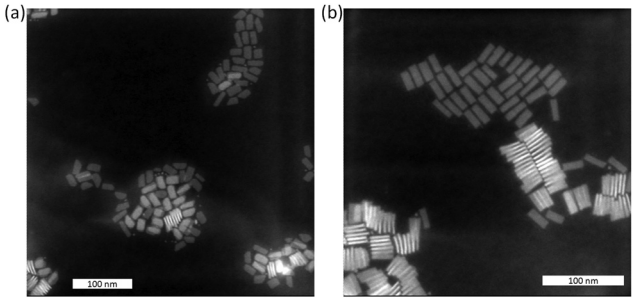

Fig. 2 HAADF-TEM images of the NPLs with (a) 4 ML having the average size of 23.57 nm (±2.90 nm) by 12.17 nm (±1.94 nm) and (b) 5 ML having the average size of 26.32 nm (±2.55 nm) by 9.04 nm (±1.41 nm). Stacking of the NPLs is clearly visible in both NPL populations. The scale bars are 100 nm.

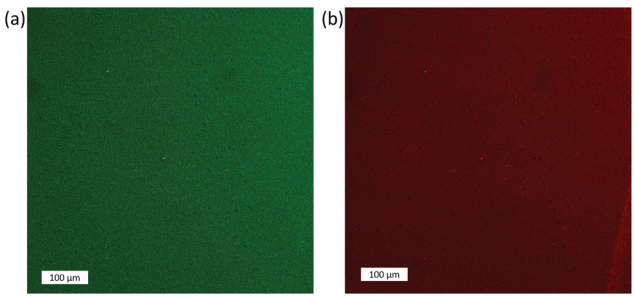

Fig. 3 Confocal images of the mixed solid films with 4 and 5 ML NPLs. The collection window is (a) 505–530 nm matching only the emission of 4 ML NPLs, and (b) 560–615 nm matching only with the emission of 5 ML NPLs. In both images, artificial coloring was used to represent the emission intensity. The scale bar is 100 μm.

is 23.57 nm (±2.90 nm) by 12.17 nm (±1.94 nm), and that of 5 ML NPLs is 26.32 nm (±2.55 nm) by 9.04 nm (±1.41 nm). Both NPLs were observed to form stacks on the TEM grids, as can be observed in Fig. 2, which has been previously demonstrated in the literature.[11,19] Stacking of the NPLs can be intentionally triggered *via* the addition of a polar solvent such as ethanol into the apolar solvent containing the NPLs, or can also be favored during the solid film formation process. Bending of the NPLs is not expected to alter its excitonic properties owing to the strong quasi-one-dimensional quantum confinement and mechanical flexibility of the NPLs.[11]

NPLs were transferred onto solid thin films *via* spin-coating them onto pre-cleaned quartz substrates. The surface coverage and homogeneity of the mixed NPL thin film samples were inspected *via* confocal microscopy using a pump laser as the Ar-ion laser line at 458 nm, which can pump both of the NPL populations simultaneously. Fig. 3 presents an exemplary case of a mixed thin film sample with an acceptor-to-donor molar ratio of 0.28. Fig. 3a shows the confocal image of the sample when the collection channel is located in the spectral range of 505–530 nm matching only the emission of 4 ML NPLs. Fig. 3b shows the confocal image of the same location of the same sample when the collection channel is located in the spectral range of 560–615 nm matching only the emission of 5 ML

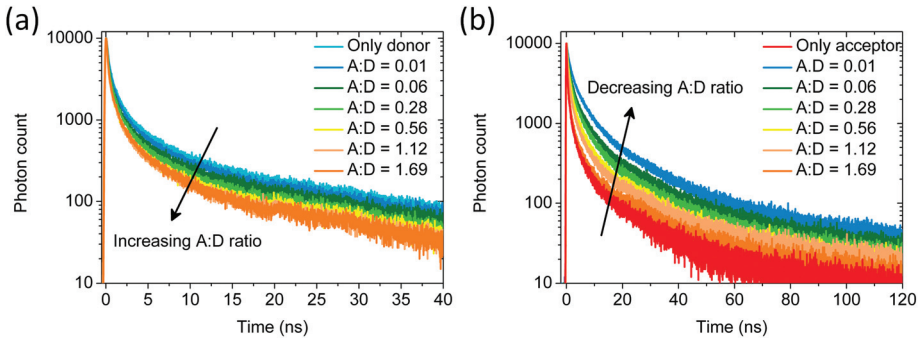

Fig. 4 Time-resolved fluorescence spectroscopy of (a) 4 ML and (b) 5 ML NPLs in their solid thin films.

NPLs. Both confocal images indicate very high surface coverage and film uniformity owing to the observation of homogenous emission all around the sample surface except a few brighter spots indicating aggregation. Therefore, the spin-coated samples were highly homogenous on the microscale. However, as we will discuss further, we observed stacking of the NPLs *via* TEM imaging leading to a nanoscale phase separation between the 4 and 5 ML NPLs.

For the NRET study, we prepared eight solid thin film samples. Two of these were the donor only and acceptor only reference samples and rest of them were mixed samples with different acceptor-to-donor (A : D) molar ratios. We then performed time-resolved fluorescence spectroscopy on these samples as shown by the fluorescence decay curves in Fig. 4. Fig. 4a and 4b depict the fluorescence decay curves of the 4 and 5 ML NPLs, respectively, for different samples with varying A : D ratio, which is calculated using the Beer–Lambert law. The concentration of the donor and acceptor NPLs is calculated to be 7.976×10^{-7} and 4.493×10^{-8} M using absorption cross sections (at 3.1 eV) of 3.1×10^{-14} and 2.5×10^{-13} cm^2, respectively.[10,20] In Fig. 4a, as the A : D ratio is increased, the donor NPLs are observed to decay faster. This indicates a new decay channel, of energy transfer, being opened up for the donor NPLs as the density of the acceptor NPLs is increased. In the case of decay kinetics for the acceptor 5 ML NPLs, we observe that the fluorescence decay is slowed down when compared to the decay of the acceptor only solid film. As frequently observed for colloidal quantum dot based acceptors, elongation of the fluorescence decay indicates the presence of exciton feeding *via* NRET into the acceptor material.[21] The rise component of the fluorescence decay in the acceptor NPLs does not significantly change upon mixing with donor NPLs since acceptor NPLs are individually strongly excited *via* absorption of the pulsed pump laser at 375 nm.

The fluorescence decay of the NPLs exhibits multi-exponential decay behavior, which was attributed to the complex decay kinetics of these materials.[10] Generally, three or four exponential decay functions were employed in the literature to fit the fluorescence decay of NPLs. In this work, we employ four exponential decay functions and fit the fluorescence decay curves in Fig. 4 with near unity reduced χ^2 and uniform residuals (see Tables S1 and S2† for the fluorescence lifetime components

Table 1 Amplitude averaged fluorescence lifetimes of the donor and acceptor NPLs for samples with various A : D ratio's. Predicted NRET rates (ns^{-1}) are also presented

Acceptor–donor ratio (A : D)							
	Donor only (or acceptor)	0.01	0.06	0.28	0.56	1.12	1.69
τ_{donor} (ns)	1.18	1.02	0.84	0.78	0.57	0.49	0.54
$\tau_{acceptor}$ (ns)	0.66	4.13	2.59	2.15	1.79	1.47	0.83
NRET Rate (ns^{-1})	—	0.133	0.343	0.435	0.907	1.193	1.00

and their fractional contribution). A possible approach to handle multi-exponential decay kinetics is to use amplitude averaged fluorescence lifetimes, although this does not fully capture the individual decay kinetics. Previously, amplitude averaged fluorescence lifetimes were also employed to investigate the NRET kinetics in the case of donors with intrinsic multi-exponential decay channels.[22] Therefore, for further analysis of the NRET rates and efficiencies, we employed the amplitude averaged fluorescence lifetimes presented in Table 1. As shown in Tables S1 and S2,† all of the fluorescence decay components were altered due to NRET. This suggests that all of the complex fluorescence decay channels are affected due to the presence of nonradiative energy transfer. As the A : D ratio is increased from 0.01 to 1.69 (Fig. 4a), we observe that the donor fluorescence decay curves become progressively faster (*i.e.*, the fluorescence lifetime of the donor NPLs decreases). This can be explained by an increase in the number of the acceptor NPLs per donor NPL. It is also important to note that for A : D ratios above 0.56, we observe that the donor decay curves do not change noticeably. This indicates a saturation of the NRET process between these donor–acceptor pairs. In the case of the acceptor decay shown in Fig. 4b, the acceptor lifetime is elongated up to 6-fold (see Table 1) in the case of small A : D ratios, where there are a large number of donor NPLs per acceptor NPL. As the A : D ratio is increased, the acceptor decays converge to the decay of the acceptor only thin film since the number of donors per acceptor was considerably decreased. Therefore, most of the acceptors are excited directly *via* the pump laser without NRET, although all of the available donor NPLs, which are less in number, are

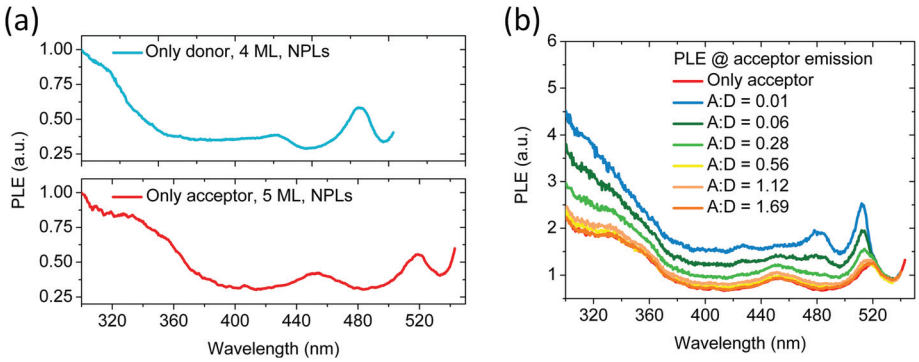

Fig. 5 (a) Photoluminescence excitation spectra for the 4 and 5 ML NPLs featuring the electron/light–hole and continuum bands. (b) Enhancement of the 5 ML NPL PLE owing to the NRET from the 4 ML NPLs.

transferring at a maximum rate. This shows that, from the acceptor point of view, exciton feeding becomes insignificant at high A : D ratios. As shown in Table 1, the NRET rates were also calculated for different A : D ratios, where the predicted NRET rate can be as high as 1.193 ns^{-1}.

Moreover, we employed photoluminescence excitation (PLE) spectroscopy to investigate the steady state evidence of NRET in these mixed NPL solid thin films. We measured the PLE spectra of the donor only and acceptor only thin film samples while monitoring the peak emission wavelength of the 4 and 5 ML NPLs, respectively, as shown in Fig. 5a. These PLE spectra highly resemble the absorption spectra of these NPLs (see Fig. 1). Spectral features observed at 480 and 518 nm correspond to the electron/light–hole transitions in the 4 and 5 ML NPLs, respectively. Fig. 5b shows the evolution of the PLE curves measured at the peak emission wavelength of the acceptor (5 ML NPLs), as the A : D ratio of the mixed samples changed from 0.01 to 1.69, together with the PLE of the acceptor only sample. Here, we normalize the PLE curves at 530 nm, since there is no contribution from the donor NPLs at this wavelength (*i.e.*, neither absorption or emission). In Fig. 5b, at small A : D ratios, where there are a large number of donors per acceptor, we observe emerging spectral features in the PLE spectrum for the acceptor emission, which is attributed to the NRET from the donor NPLs.

To understand the origin of the newly emerged spectral features in Fig. 5b, we calculated the spectral enhancement of the PLE curves in the mixed samples normalized with respect to the acceptor only sample. The resulting curves are presented in Fig. 6. We observe that the spectral enhancement resembles the PLE spectra of the donor NPLs. The features observed around 510 and 480 nm correspond to the electron/heavy–hole and electron/light–hole transitions in the donor 4 ML NPLs. This indicates that across the spectral range where the donor NPLs are better excited, the energy transfer into the acceptor NPLs becomes stronger and more efficient. In addition, at the higher photon energy tail of the 480 nm peak, there is enhancement of the PLE due to the continuum absorption states of the donor NPLs. The largest enhancement of the PLE of the acceptor NPLs is achieved when the donors are 100× the acceptors (corresponding to the A : D ratio of 0.01) due to the presence of abundant donor NPLs increasing the probability of the funneling excitons into the acceptor NPLs. At small A : D ratios, the dominant excitation mechanism of the acceptor NPLs is through NRET since a PLE enhancement factor of up to 2.8-fold could be achieved. As the A : D ratio is increased, we observe that the enhancement of PLE gradually diminishes since the number of donors per acceptor is concomitantly decreased. At these large A : D ratios, the acceptor NPLs are dominantly excited *via* the pump light instead of being excitonically pumped by NRET from the donor NPLs since the PLE enhancement factor is close to 1 in this range.

Fig. 7 shows the NRET efficiency as a function of the A : D ratio as computed as follows:

$$\gamma_{\text{donor}} = \gamma_{\text{radiative}} + \gamma_{\text{nonradiative}} \quad (1)$$

$$\gamma_{\text{donor\_with\_acceptor}} = \gamma_{\text{radiative}} + \gamma_{\text{nonradiative}} + \gamma_{\text{NRET}} \quad (2)$$

$$\eta_{\text{NRET}} = 1 - \frac{\tau_{\text{donor\_with\_acceptor}}}{\tau_{\text{donor}}} \quad (3)$$

Here, $\gamma_{\text{donor}}\left(=\frac{1}{\tau_{\text{donor}}}\right)$ is the fluorescence decay rate of the donor NPLs in the absence of acceptors. $\gamma_{\text{radiative}}$ and

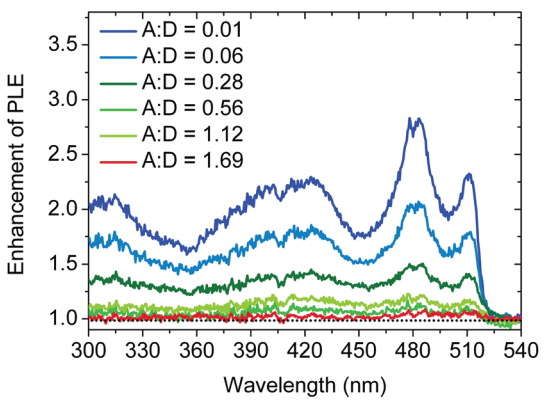

Fig. 6 Enhancement of the acceptor NPL emission excitation exhibiting spectral features resembling the spectral PLE features of the donor NPLs. At small A : D ratios, the dominant excitation mechanism of the acceptor NPLs is through NRET, whereas at large A : D ratios the acceptor NPLs are dominantly excited through direct absorption of the pump photons.

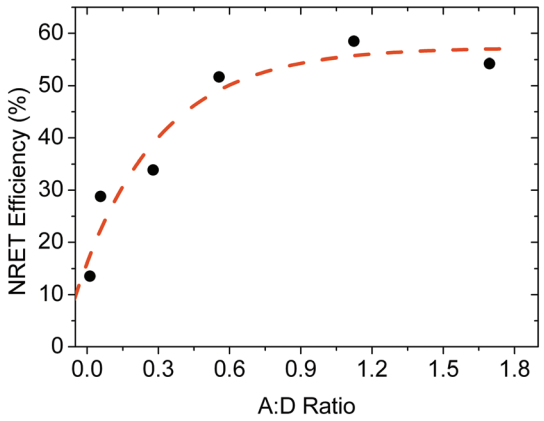

Fig. 7 NRET efficiency as a function of the A : D ratio.

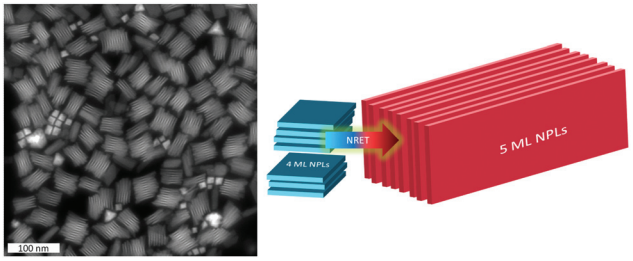

Fig. 8 A HAADF-TEM image of the mixed NPL assembly (without size selective precipitation) of square-like 4 ML NPLs and rectangle-like 5 ML NPLs. A schematic representation of the NRET as limited by the nanoscale phase segregation between the NPLs of different populations.

$\gamma_{\text{nonradiative}}$ are the intrinsic radiative and nonradiative decay rates of the donor NPLs, respectively. $\gamma_{\text{donor\_with\_acceptor}}\left(=\frac{1}{\tau_{\text{donor\_with\_acceptor}}}\right)$ is the fluorescence decay rate of the donor NPLs in the presence of acceptors. γ_{NRET} is the rate of the NRET process and η_{NRET} is the efficiency of the NRET. Because of the architecture and dimensionality of the NPLs, the NRET efficiency is expected to be large since close-packing in NPL assemblies would be achieved owing to the small magic sized vertical thickness (3 ML ~0.9 nm, 4 ML ~1.2 nm, 5 ML ~1.5 nm) of the NPLs. In this work, however, NRET efficiencies are observed to be limited to 60% as given in Fig. 7. Based on coulombic dipole–dipole coupling, we compute the Förster radius[22] to be 10.83 nm between the donor–acceptor pairs using the following parameters. The extinction coefficient of 5 ML NPLs at 500 nm is calculated to be 4.86×10^7 M^{-1} cm^{-1}, the quantum yield of the donor NPLs is 10%, the dipole orientation factor (κ^2) is 2/3 assuming random transition dipole orientations and the refractive index of the medium is 1.8. If the 4 and 5 ML NPLs were to perfectly assemble in the form of inter-mixed stacks (similar to two bunches of poker cards that are mixed well together), then the donor-to-acceptor separation distance would be expected to be comparable to 4–5 nm on average due to interpenetrating ligands as previously demonstrated by small-angle X-ray scattering measurements (SAXS).[11,19] Therefore, NRET greater than 95% would have been possible in these solid films in the case of perfect inter-stacking. On the other hand, we experimentally observe the saturation of the NRET efficiencies below such a high efficiency level.

To understand the possible reason for this limited NRET, we now synthesize 5 ML NPLs that intentionally contain ~5% of 4 ML NPLs as a side product of the synthesis (*i.e.*, a mixed NPL solution containing 5 ML NPLs with a population of ~95%). This time we did not perform size selective precipitation so that these mixed NPL populations stay together. Then, we casted the mixed solution on TEM grids to investigate their solid film assemblies *via* TEM imaging. Here, the 4 ML NPLs have a square-like shape with an average size of 10.81 nm (±0.53 nm) and the 5 ML NPLs have a rectangle-like shape with an average size of 43.67 nm (±3.31 nm) and 12.94 nm (±1.51 nm) (see Fig. S1†). We observe severe stacking of the NPLs within their own population. Fig. 8 demonstrates the HAADF-TEM image of the mixed solid film together with a representative cartoon to illustrate the limitation of the NRET process resulting from the nanoscale phase segregation between the donor and acceptor NPL populations due to their self-stacking. Here NRET is found to be limited with the longer lateral size of the NPLs, which is in the order of 10 nm, since it is not possible to achieve inter-mixed stacked assemblies of the different populations of NPLs, but instead the mixture of the self-stacked assemblies. Due to this nanoscale phase segregation, NRET efficiencies are limited to ~60% corresponding to an almost average separation about the Förster radius (*i.e.*, 10.83 nm), which matches well with the center-to-center separation of 10.61 nm (0.5 × 12.17 nm + 0.5 × 9.04 nm) between two adjacent donor and acceptor NPLs. A similar type of phase segregation has also been observed in the conjugated polymer – colloidal quantum dot based hybrids limiting the NRET in those organic—inorganic assemblies.[23,24] Due to this larger separation between the donor and acceptor species, higher order multi-polar interactions are not expected to be significant.[25]

In summary, we have demonstrated the first account of spectral evidence for nonradiative energy transfer in solid thin film assemblies incorporating colloidal CdSe nanoplatelets with different vertical thicknesses. Both steady state and time-resolved fluorescence spectroscopy proves that excitons generated in the donor, 4 ML thick NPLs can be funneled into the acceptor, 5 ML thick NPLs *via* near field dipole–dipole coupling. The efficiency of NRET can reach 60%, however, further increase in the efficiency is limited by the nanoscale phase segregation between the donor and acceptor NPL populations due to the self-stacking of the NPLs within their own populations leading to increased distance between the donor–acceptor pairs. This type of nanoscale phase separation has not been observed in mixed solid films of the quantum dots and nanorods to date. As future work, we are developing inter-stacked NPL assemblies of mixed populations to boost the NRET efficiency in NPL assemblies.

Experimental section

Synthesis of the 4 ML NPLs

For a typical synthesis, 170 mg of cadmium myristate, 12 mg of selenium and 15 mL of octadecene (ODE) were loaded into a three-neck flask. After evacuation of the mixed solution at room temperature, it was heated to 240 °C under an inert atmosphere. When the temperature reaches 195 °C, the color of solution becomes yellowish. Then, 80 mg of cadmium acetate dihydrate was introduced. After 10 min growth of the CdSe NPLs at 240 °C, the reaction was stopped and cooled down to room temperature with injection of 0.5 mL of oleic acid (OA). The resulting 4 ML CdSe NPLs were separated from the other reaction products with successive purification steps.

Synthesis of the 5 ML NPLs

170 mg of cadmium myristate and 15 mL of ODE were loaded into a three-neck flask. After evacuation of solution at room temperature, the solution was heated to 250 °C under an inert atmosphere. 12 mg of Se dispersed in 1 ml of ODE was swiftly injected. 80 mg of cadmium acetate dihydrate was introduced one minute later. After 10 minutes growth of CdSe NPLs at 250 °C, the reaction was stopped and cooled down to room temperature with the injection of 0.5 mL of OA. 5 ML CdSe NPLs were separated from the other reaction products with successive purification steps.

Purification and size-selective precipitation of the nanoplatelets

As-synthesized NPLs were centrifuged at 4500 rpm for 5 min. The supernatant solution was removed from the centrifuge tube. The precipitate was dried under nitrogen, dissolved in hexane and centrifuged again at 4500 rpm for 10 min. The supernatant was used for the further process. Ethanol was added into the supernatant solution until it became turbid. Then, the turbid solution was centrifuged at 4500 rpm for 10 min. The precipitate was dissolved in hexane and filtered using a 0.20 micrometer filter.

Preparation of the solid NPL thin films

The concentration of the 4 and 5 ML NPL solutions were calculated as 7.976×10^{-7} and 4.493×10^{-8} M, respectively. Samples of 4–5 ML NPL solutions having different acceptor-to-donor (A : D) molar ratios, mixed using ultrasonication for 5 min, were prepared. The quartz substrates of 1.5 by 1.5 cm in size were cleaned using piranha solution for 30 min, cleaned with DI-water and dried in an oven at 80 °C for 30 min. The mixed NPL solid thin films were prepared using spin-coating the mixed solutions at 2000 rpm for 1 min.

Steady state and time-resolved optical characterization

Steady state photoluminescence spectra and photoluminescence excitation spectra were collected using a Cary Eclipse Fluorescence Spectrometer. Photoluminescence quantum yield measurements were performed in the solution phase using Rhodamine 6G as the reference dye. Confocal microscopy images were collected using a Zeiss LSM 510. An Ar laser line at 458 nm was employed as the excitation source for the confocal imaging. Time-resolved fluorescence decay kinetics were measured using PicoQuant FluoTime 200 that employs PicoHarp 300 time-correlated single photon counting (TCSPC) unit and a picosecond pump laser at 375 nm. Fluorescence decay curves were fitted using the FluoFit program with multi-exponential decay functions.

Acknowledgements

The authors would like to thank the financial support from EU-FP7 Nanophotonics4Energy NoE, TUBITAK EEEAG 109E002, 109E004, 110E010, 110E217, NRF-RF-2009-09, NRF-CRP-6-2010-02 and A*STAR of Singapore. H. V. D. acknowledges the support from ESF-EURYI and TUBA-GEBIP.

References

1 S. Ithurria and B. Dubertret, *J. Am. Chem. Soc.*, 2008, **130**, 16504–16505.
2 S. Ithurria, M. D. Tessier, B. Mahler, R. P. S. M. Lobo, B. Dubertret and A. L. Efros, *Nat. Mater.*, 2011, **10**, 936–941.
3 M. D. M. D. Tessier, C. Javaux, I. Maksimovic, V. Loriette, B. Dubertret, L. T. Kunneman, H. Heuclin, Y. V. Aulin, F. C. Grozema, J. M. Schins and L. D. A. Siebbeles, *J. Phys. Chem. Lett.*, 2013, **4**, 3574–3578.
4 M. D. Tessier, B. Mahler, B. Nadal, H. Heuclin, S. Pedetti and B. Dubertret, *Nano Lett.*, 2013, **13**, 3321–3328.
5 A. W. Achtstein, A. Schliwa, A. Prudnikau, M. Hardzei, M. V. Artemyev, C. Thomsen and U. Woggon, *Nano Lett.*, 2012, **12**, 3151–3157.
6 M. Pelton, S. Ithurria, R. D. Schaller, D. S. Dolzhnikov and D. V. Talapin, *Nano Lett.*, 2012, **12**, 6158–6163.
7 Z. Chen, B. Nadal, B. Mahler, H. Aubin and B. Dubertret, *Adv. Funct. Mater.*, 2014, **24**, 295–302.
8 B. Guzelturk, Y. Kelestemur, M. Olutas, S. Delikanli and H. V. Demir, *ACS Nano*, 2014, **8**, 6599–6605.
9 C. Bouet, M. D. Tessier, S. Ithurria, B. Mahler, B. Nadal and B. Dubertret, *Chem. Mater.*, 2013, **25**, 1262–1271.
10 M. D. Tessier, C. Javaux, I. Maksimovic, V. Loriette and B. Dubertret, *ACS Nano*, 2012, **6**, 6751–6758.
11 M. D. Tessier, L. Biadala, C. Bouet, S. Ithurria, B. Abecassis and B. Dubertret, *ACS Nano*, 2013, **7**, 3332–3340.
12 L. T. Kunneman, M. D. Tessier, H. Heuclin, B. Dubertret, Y. V. Aulin, F. C. Grozema, J. M. Schins, L. D. A. Siebbeles, D. Cdse, C. Cdzns and C. Shell, *J. Phys. Chem. Lett.*, 2013, **4**, 3574–3578.
13 L. Biadala, F. Liu, M. D. Tessier, D. R. Yakovlev, B. Dubertret and M. Bayer, *Nano Lett.*, 2014, **14**, 1134–1139.
14 T. Förster, *Ann. Phys.*, 1948, **437**, 55–75.
15 B. Guzelturk, P. L. H. Martinez, Q. Zhang, Q. Xiong, H. Sun, X. W. Sun, A. O. Govorov and H. V. Demir, *Laser Photonics Rev.*, 2014, **8**, 73–93.

16 A. L. Rogach, *Nano Today*, 2011, **6**, 355–365.
17 A. R. Clapp, I. L. Medintz and H. Mattoussi, *ChemPhysChem*, 2006, **7**, 47–57.
18 A. Yeltik, B. Guzelturk, P. L. Hernandez-Martinez, A. O. Govorov and H. V. Demir, *ACS Nano*, 2013, **7**, 10492–10501.
19 B. Abécassis, M. D. Tessier, P. Davidson and B. Dubertret, *Nano Lett.*, 2014, **14**, 710–715.
20 C. She, I. Fedin, D. S. Dolzhnikov, A. Demortière, R. D. Schaller, M. Pelton, D. V. Talapin and D. Richard, *Nano Lett.*, 2014, **14**, 2772–2777.
21 C. Kagan, C. Murray, M. Nirmal and M. Bawendi, *Phys. Rev. Lett.*, 1996, **76**, 1517–1520.
22 J. R. Lakowicz, *Principles of Fluorescence Spectroscopy*, Springer US, Boston, MA, 2006, vol. 13.
23 T. Stoferle, U. Scherf and R. F. Mahrt, *Nano Lett.*, 2009, **9**, 453–456.
24 B. Guzelturk, P. L. Hernandez Martinez, V. K. Sharma, Y. Coskun, V. Ibrahimova, D. Tuncel, A. Govorov, X. Sun, Q. Xiong and H. V. Demir, *Nanoscale*, 2014, **6**, 11387–11394.
25 T. W. J. Gadella, *Fret and Flim Techniques*, Elsevier, 2009, vol. 33.